



POLITECNICO
MILANO 1863

Politecnico di Milano

Smart structures and devices: report

Energy harvesting and bandgap creation on a cantilever beam through the use of
piezoelectrics and metamaterials

Max Derie – Hans Agger Hougaard

Contents

List of figures	2
List of tables.....	2
1. Introduction	3
2. Background	4
2.1. Piezoelectricity	4
2.2. Metamaterials.....	5
3. Problem description.....	6
4. Theory - Cantilevered Beam	7
5. Theory - Cantilever with Resonators and Uniform Piezo Elements	10
5.1. Simple Beam Governing Equation.....	11
5.2. Resonator Governing Equation	12
5.3. Bending Stress in the Piezo Elements	12
5.4. Piezo Electric Potential Equation	14
5.5. Further Derivation of the Beam Equation.....	15
5.6. Assuming Harmonic Solutions.....	17
6. Numerical simulation of beam.....	21
7. Study of beam parameters	25
7.1. Influence of mass ratio.....	25
7.2. Influence of Number of Resonators on Bandgap Formation	26
7.3. Influence of resonator damping ratio	27
7.4. Choice of piezoelectric material.....	28
7.5. Thickness of the Piezo Elements	29
7.6. Influence of load resistance	31
7.7. Comparison to initial guess	32
8. Conclusion.....	34
9. Outlook	35
References	36

List of figures

Figure 1: Schematic depiction of the Piezoelectric effect (Fleischer, 2019)	4
Figure 2: metamaterial with resonators (Erturk, 2019).....	5
Figure 3: schematic of the cantilever beam	11
Figure 4: Total tip displacement	22
Figure 5: Total tip displacement of simple cantilever beam.....	22
Figure 6: resonator and beam deflections.....	22
Figure 7 Absolute beam deflection at antiresonance frequency	23
Figure 8: Generated power.....	23
Figure 9: Influence of mass ratio on bandgap	25
Figure 10: Effect of varying resonator amount.....	26
Figure 11: Influence of resonator damping	27
Figure 12: Different piezoelectric materials on tip displacement	28
Figure 13: Different piezoelectric materials on harvested power	28
Figure 14: Influence of Piezopatch Thickness.....	29
Figure 15: Varying piezopatch thickness in the spectrum of interest for energy harvesting	30
Figure 16: Influence of varying load on generated voltage and current	31
Figure 17: Influence varying load on power and tip displacement	32
Figure 18: Comparison between harvested power with initial guess and optimised parameters	32

List of tables

Table 1: Cantilever beam parameters	6
Table 2: Initially guessed parameters	21
Table 3: Piezoelectric material data – PZT-5A	28
Table 4: Piezoelectric material data – PZT-55.....	28
Table 5: Piezoelectric material data – PMN-PT 33%.....	28
Table 6: Initially guessed parameters	33
Table 7: Parameters after optimisation.....	33

1. Introduction

With the growing complexity of modern day physical structures and their applications, use of materials with special properties – properties that cannot be found in common construction materials such as steel – has been growing significantly. One class of materials that is known to have many ‘exotic’ characteristics that extend over a wide variety of applications, is the material family of the ceramics. One family of these ceramics is the family of piezoceramics, of which a possible application will be investigated in this report. The piezoelectric property couples a mechanical deformation to a dielectric displacement, leading to a separation of charges within the material, which can then in turn create a voltage and current, if attached to a load. This effect can potentially be used to harvest energy off of the motion of the material, if the deformations are high enough.

Together with the piezoceramics, another class of materials called metamaterials will be investigated. These are synthetically produced materials that exhibit properties commonly not found in nature. In this case, special interest goes out to the property of creating resonant structures that cancel out certain vibrations in the structure to which they are applied.

The scope of this report is to apply the two mentioned classes of materials to a vibrating cantilever beam, in order to investigate the possibilities of creating a local bandgap in the frequency spectrum, where vibrations will be cancelled out, and to harvest energy from other frequencies. This will be achieved by first clearly formulating a problem statement and the assumptions that will be made. After that, mathematical derivations will be made to demonstrate how several outputs, such as generated power and cantilever deformation, relate to the input force and piezoelectric and metamaterial interaction effects. Based on these calculations, several parameters associated to the beam, metamaterial and piezoelectric patches will be optimized with respect to the desired bandgap creation and energy harvesting. These results will be visually supported by several graphs representing the influence of the parameters on the behavior of the system.

2. Background

This segment will provide a short explanation of the workings of piezoelectric materials and metamaterials and how they can be used to achieve the desired effects in the cantilevered beam. The section is based on (Braghin, 2019).

2.1. Piezoelectricity

Piezoelectric effects occur almost solely in ionic crystal structures. These structures are made up of positively and negatively charged ions, that, when in an equilibrium state where no external stress or voltage is applied, are arranged in a way so no potential exists over the unit cell. In other terms, the charges cancel each other out. If a strain is applied to the crystal however, the unit cells deform, which alters the relative positions of the ions in the cell. Because of this displacement, a charge separation has occurred, which leads to an internal electric field being generated between the two poles. The application of strain on the piezoelectric element therefore leads to a voltage generation over the element, in a direction orthogonal to the applied strain. This effect is demonstrated in figure 1.

Piezoelectric Effect in Quartz

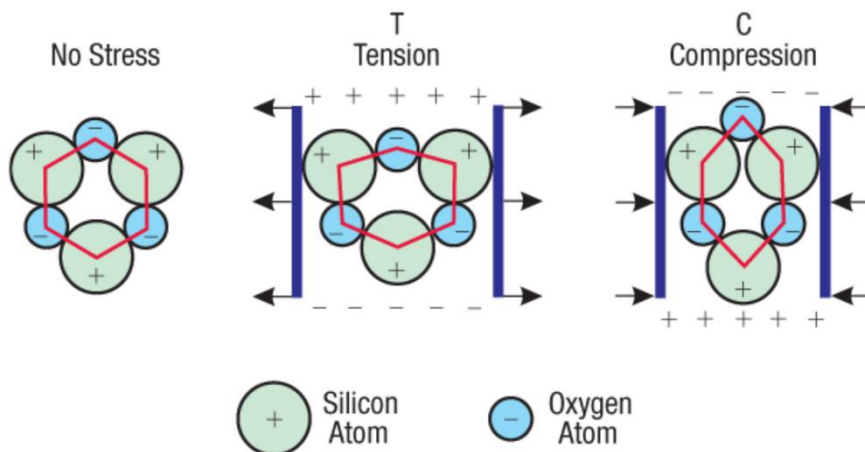


FIGURE 1: SCHEMATIC DEPICTION OF THE PIEZOELECTRIC EFFECT (FLEISCHER, 2019)

If electrodes are attached to the two sides of a piezoelectric element, and it is connected to an electric load, a current can be generated through this load by applying a varying strain to the piezoelectric element. Voltage generation through the application of stress is called the direct piezoelectric effect. Conversely, the opposite can also be achieved: by applying a varying electric field to a piezoelectric element, a vibration can be induced in the element. This is the indirect piezoelectric effect.

2.2. Metamaterials

The term ‘metamaterials’ is a group name for all synthetically produced materials that exhibit properties that are not found in naturally occurring materials (Mehdizadeh, 2009). They therefore span a wide range of different materials, properties and applications. This report will focus on metamaterials that are locally resonant, so vibrations of a certain range of frequencies will be cancelled.

This can be achieved in a purely mechanical way, by attaching a periodic structure of spring-mass elements to the material on which the vibrations must be damped (Christopher Sugino, 2016). A representation of this is given in figure 2.

By tuning the spring stiffness and resonator mass, a bandgap of desired width can be achieved, at the

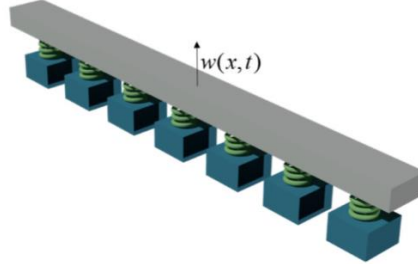


FIGURE 2: METAMATERIAL WITH RESONATORS (ERTURK, 2019)

desired frequency. The starting frequency of the bandgap is determined by the resonance frequency of the spring-mass system, as the interaction of the main material with this spring mass will be the factor that causes the local attenuation. Therefore, the expression $\omega_t = \sqrt{\frac{k_j}{m_j}}$ can be stated (Christopher Sugino, 2016), where ω_t corresponds to the starting frequency of the bandgap, and k_j and m_j are the spring stiffness and mass of the resonator respectively.

The width of the bandgap is dependent on the mass of the resonators. A lot of mass will create a large bandgap, but an overall heavier and possibly very large structure. The width of the bandgap is given by $BW = \omega_t \cdot (1 - \sqrt{1 + \mu})$, $\mu = \frac{\sum_{j=1}^N m_j}{m_{struct}}$. μ , the mass ratio, is the ratio between the total added mass of resonators and the mass of the original structure (Christopher Sugino, 2016). As can be seen, there are two tunable parameters, the resonator mass and stiffness, which can be used to tune the bandgap location and width to any liking. Instead of using conventional, constant value for the stiffness, nonlinearities can also be introduced to enhance the bandgap without adding too much mass.

This locally resonant behavior can also be achieved through a periodic structure of piezoelectric patches.

3. Problem description

The system setup of the structure that will be used in this report is that of a steel cantilever beam, clamped into a wall at one end and free at the other end. The beam is subject to a vibrating motion at its base (base motion), and the motion of the tip due to this base excitation is investigated for different excitation frequencies. The requirements for the project are:

- 1) A bandgap must be created around the fifth resonance frequency with a bandwidth of at least 50 Hz by using the locally resonant metamaterials.
- 2) A configuration of piezoelectric patches must be elaborated in order to harvest power at the edge of the bandgap. More specifically, the power harvesting will be optimised for a frequency range of 3000 – 3500 rad/s.

Throughout the solving process, the effect of the parameters coming into play will be visually demonstrated and described using graphs. The specifications of the cantilever beam are given in table 1:

Length [m]	0,5
Width [m]	0,01
Thickness [m]	0,003
E-modulus [GPa]	200
density [kg/m ³]	7800

TABLE 1: CANTILEVER BEAM PARAMETERS

Other parameters, relating to the beam, resonator or piezoelectric elements, are all parameters that can be altered to enhance the bandgap and energy harvesting process.

4. Theory - Cantilevered Beam

This section gives a brief theoretical derivation of the behavior of a cantilevered beam used for the case study of the report. It is based entirely on classroom presentations and the supplied appendix (Inman, Piezoelectric Energy Harvesting - Appendix C Modal Analysis of a Uniform Cantilever with a Tip Mass, 2011) from the course “Smart Structures and Devices 2018/19” at Politecnico Di Milano.

Euler Bernoulli beam theory for an unforced beam states that.

$$YI \frac{\partial^4 w(x, t)}{\partial x^4} + m \frac{\partial^2 w(x, t)}{\partial t^2} = 0$$

Where m is mass per length, I is the area moment of inertia, Y is Young's modulus and $w(x, t)$ is the transverse displacement. The equation is a homogeneous partial differential equation as there is no forcing term included. The equation can only be solved for the homogeneous solution, while for the case study of this report only the steady state response is of interest. However, it can be shown that the mode shapes of the general solution are also the mode shapes of the particular solution.

A solution for the transverse displacement is sought after as a combination of a function of time and a function of space. The solution is sought after using separation of variables. (Inman, Piezoelectric Energy Harvesting - Appendix C Modal Analysis of a Uniform Cantilever with a Tip Mass, 2011).

$$w(x, t) = \phi(x)\eta(t)$$

$$YI \frac{\partial^4 \phi(x)\eta(t)}{\partial x^4} + m \frac{\partial^2 \phi(x)\eta(t)}{\partial t^2} = 0 \Leftrightarrow \frac{YI}{m} \frac{1}{\phi(x)} \frac{\partial^4 \phi(x)}{\partial x^4} = -\frac{1}{\eta(t)} \frac{\partial^2 \eta(t)}{\partial t^2} = k$$

Since the two sides of the equation are functions of independent variables, they must both be constant for any variation.

$$\Rightarrow \phi'''(x) - C\phi(x) = 0, \ddot{\eta}(t) + k\eta(t) = 0$$

where

$$C = \frac{km}{YI}$$

It is shown that k must be positive for an oscillatory response.

$$k = 0 \Rightarrow \ddot{\eta}(t) + k\eta(t) = 0 \Rightarrow \ddot{\eta}(t) = 0 \Rightarrow \eta(t) = Ax + B$$

$$k < 0, \omega^2 = -k \Rightarrow \ddot{\eta}(t) + k\eta(t) = 0 \Rightarrow \ddot{\eta}(t) = \omega^2\eta(t) \Rightarrow \eta(t) = Ae^{\omega t}$$

$$k > 0, \omega^2 = k \Rightarrow \ddot{\eta}(t) + k\eta(t) = 0 \Rightarrow \ddot{\eta}(t) = -\omega^2\eta(t) \Rightarrow \eta(t) = A\cos(\omega t) + B\sin(\omega t)$$

Therefore, $C > 0$, $\frac{\omega^2 m}{YI} = C$ and any of the following four functions are solutions to the ODE. The solutions are superposed.

$$\phi'''(x) = \frac{\omega^2 m}{YI} \phi(x) \Rightarrow \phi(x) = A \sin\left(\sqrt[4]{\frac{\omega^2 m}{YI}} x\right) + B \cos\left(\sqrt[4]{\frac{\omega^2 m}{YI}} x\right) + C \sinh\left(\sqrt[4]{\frac{\omega^2 m}{YI}} x\right) + D \cosh\left(\sqrt[4]{\frac{\omega^2 m}{YI}} x\right)$$

A variable λ is introduced

$$\lambda^4 = \frac{\omega^2 m L^4}{YI}$$

$$\phi(x) = A \sin\left(\frac{\lambda}{L} x\right) + B \cos\left(\frac{\lambda}{L} x\right) + C \sinh\left(\frac{\lambda}{L} x\right) + D \cosh\left(\frac{\lambda}{L} x\right)$$

The Boundary conditions for the cantilevered beam are

$$w(0, t) = 0, \frac{\partial w(0, t)}{\partial x} = 0, \frac{\partial^2 w(L, t)}{\partial x^2} = 0, \frac{\partial^3 w(L, t)}{\partial x^3} = 0$$

Except for the trivial case of $\eta(t) = 0$ the first two boundary conditions at the clamped end can be reformulated as.

$$\phi(0) = 0, \left. \frac{\partial \phi}{\partial x} \right|_{x=0} = 0$$

This gives

$$A \sin(0) + B \cos(0) + C \sinh(0) + D \cosh(0) = 0 \Leftrightarrow B = -D$$

$$A \frac{\lambda}{L} \cos(0) - B \frac{\lambda}{L} \sin(0) + C \frac{\lambda}{L} \cosh(0) + D \frac{\lambda}{L} \sinh(0) = 0 \Leftrightarrow A = -C$$

Similarly, for the boundary conditions at the tip.

$$\left. \frac{\partial^2 \phi}{\partial x^2} \right|_{x=L} = 0$$

\Rightarrow

$$-\frac{\lambda^2}{L^2} A \sin(\lambda) - \frac{\lambda^2}{L^2} B \cos(\lambda) - \frac{\lambda^2}{L^2} A \sinh(\lambda) - \frac{\lambda^2}{L^2} B \cosh(\lambda) = 0$$

\Leftrightarrow

$$B = -A \frac{\sin(\lambda) + \sinh(\lambda)}{\cos(\lambda) + \cosh(\lambda)}$$

$$\left. \frac{\partial^3 \phi}{\partial x^3} \right|_{x=L} = 0$$

\Rightarrow

$$-A \cos(\lambda) - A \frac{\sin(\lambda) + \sinh(\lambda)}{\cos(\lambda) + \cosh(\lambda)} \sin(\lambda) - A \cosh(\lambda) + A \frac{\sin(\lambda) + \sinh(\lambda)}{\cos(\lambda) + \cosh(\lambda)} \sinh(\lambda) = 0$$

The final constant A is simply a scaling of ϕ relative to η and can be selected arbitrarily. To solve for λ it's set to 1.

$$-\cos(\lambda) - \frac{\sin(\lambda) + \sinh(\lambda)}{\cos(\lambda) + \cosh(\lambda)} \cdot \sin(\lambda) - \cosh(\lambda) + \frac{\sin(\lambda) + \sinh(\lambda)}{\cos(\lambda) + \cosh(\lambda)} \sinh(\lambda) = 0$$

\Rightarrow

$$\lambda_{1..10} = \{1.875, 4.694, 7.854, 10.996, 14.135, 17.278, 20.42, 23.56, 26.704, 29.845\}$$

This yields an infinite series of solutions. The deflection of the beam is therefore a combination of these. To be able to compute, a finite amount of 10 modeshapes are considered. After significantly high frequencies are reached in $\eta_r(t)$ the series is truncated as higher frequencies will have little or no resonance. Combining the solutions found with separation of variables gives.

$$w(x, t) = \sum_{r=1}^n \phi_r(x) \eta_r(t)$$

Remembering the constant solutions from the BC's and defining a new constant σ_r

$$B = -D, A = -C, B = -A \frac{\sin(\lambda) + \sinh(\lambda)}{\cos(\lambda) + \cosh(\lambda)} = -A \sigma_r$$

The equation is reformulated with the new constant.

$$\begin{aligned} \phi(x) &= A \sin\left(\frac{\lambda}{L}x\right) + B \cos\left(\frac{\lambda}{L}x\right) + C \sinh\left(\frac{\lambda}{L}x\right) + D \cosh\left(\frac{\lambda}{L}x\right) = \\ &= A \left(\sin\left(\frac{\lambda}{L}x\right) - \sinh\left(\frac{\lambda}{L}x\right) + \sigma_r \left(\cosh\left(\frac{\lambda}{L}x\right) - \cos\left(\frac{\lambda}{L}x\right) \right) \right) \end{aligned}$$

It can be shown that selecting $A = \sqrt{\frac{1}{mL}}$ will yield the following orthogonality condition. A similar result and procedure with different boundary conditions is demonstrated in (Inman, Piezoelectric Energy Harvesting - Appendix C Modal Analysis of a Uniform Cantilever with a Tip Mass, 2011).

$$\int_0^L \phi_s(x) m \phi_r(x) dx = \delta_{rs}$$

⇒

$$\int_0^L \phi_s(x) YI \frac{\partial^4 \phi_r(x)}{\partial x^4} dx = \int_0^L \phi_s(x) YI \frac{\lambda^4}{L^4} \phi_r(x) dx = YI \int_0^L \phi_s(x) \omega^2 m \phi_r(x) dx = \omega^2 \delta_{rs}$$

With these orthogonality conditions the necessary derivations for the case study can be made.

5. Theory - Cantilever with Resonators and Uniform Piezo Elements

In this section equations governing a beam with a uniform piezo patch and attached resonators are derived. Derivations are made to solve it using matrix operations. The derivations are based on linearity and separation of variables. It is assumed that the time independent solution to the beam equation is unaffected by both piezo-elements and resonators. The section is based on (Christopher Sugino, 2016) and (Inman, Piezoelectric Energy Harvesting - Analytical Distributed-Parameter Electromechanical Modeling of Cantilevered Piezoelectric Energy Harvesters First Edition., 2011)

Figure 3 depicts a schematic of the cantilever beam, to which resonators and piezoelectric materials are fitted. On the figure, the grey element represents the steel cantilever beam, while the red elements attached on the top and bottom side are the piezoelectric patches, connected in series to a circuit with load R_L . The individual degrees of freedom are the forced base motion w_{base} , the beam deflection relative to the base motion w_{rel} and the resonators displacement u_j relative to the location where they're attached. The resonators are attached with spring dampers with spring coefficient k_j and damping coefficients c_j . It is assumed that the beam operates in vacuum and that the Piezo elements have perfect adhesion to the beam.

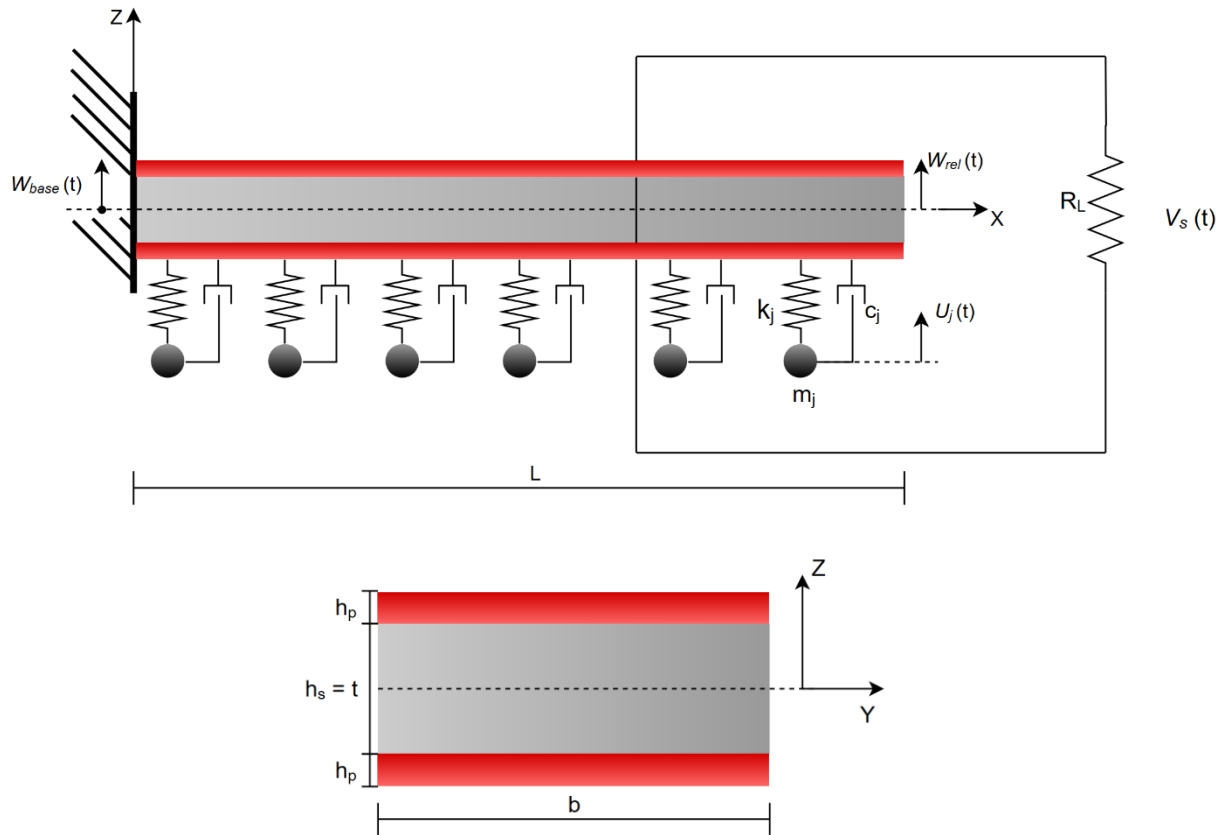


FIGURE 3: SCHEMATIC OF THE CANTILEVER BEAM

5.1. Simple Beam Governing Equation

With Euler Bernoulli beam theory, the beam without piezo elements or resonators can be expressed as.

$$-\frac{\partial^2 M}{\partial x^2} + m \frac{\partial^2 w}{\partial t^2} = f_{ext}(x, t)$$

Where M is the bending moment, m is the mass per length, w is displacement and f is the external force.

Damping terms are included with damping coefficients c_s, c_e .

$$-\frac{\partial^2 M}{\partial x^2} + c_s I \frac{\partial^5 w}{\partial x^4 \partial t^1} + c_e \frac{\partial w}{\partial t} + m \frac{\partial^2 w}{\partial t^2} = f_{ext}(x, t)$$

The absolute displacement is separated into base motion term and a displacement relative to the base motion.

$$w = w_b + w_{rel}$$

The beam equation is expressed using this.

$$-\frac{\partial^2 M}{\partial x^2} + c_s I \frac{\partial^5 w_{rel}}{\partial x^4 \partial t^1} + c_e \frac{\partial w_{rel}}{\partial t} + m \frac{\partial^2 w_{rel}}{\partial t^2} = -c_s \frac{\partial^5 w_b}{\partial x^4 \partial t^1} - c_e \frac{\partial w_b}{\partial t} - m \frac{\partial^2 w_b}{\partial t^2} + f_{ext}(x, t)$$

The damping on base motion is ignored as the base motion is induced and considered unaffected by beam dynamics.

$$-\frac{\partial^2 M}{\partial x^2} + c_s I \frac{\partial^5 w_{rel}}{\partial x^4 \partial t^1} + c_e \frac{\partial w_{rel}}{\partial t} + m \frac{\partial^2 w_{rel}}{\partial t^2} = -m \frac{\partial^2 w_b}{\partial t^2} + f_{ext}(x, t)$$

5.2. Resonator Governing Equation

The j 'th resonator's governing equation is expressed with its DoF u_j , relative to the beam at the position where it's attached. Using Newton's second law the absolute displacements of the resonator masses now have three terms.

$$\left(\ddot{u}_j + \frac{\partial^2}{\partial t^2} w_{rel}(x_j, t) + \dot{w}_b \right) \cdot m_j = -u_j k - c \cdot \dot{u}_j$$

Where k is the spring constant and c is the damper coefficient.

\Leftrightarrow

$$\ddot{u}_j + 2 \cdot \zeta \cdot \omega_0 \dot{u}_j + \omega_0^2 u_j + \frac{\partial^2 w_{rel}(x_j, t)}{\partial t^2} = -\dot{w}_b$$

Where the damping ratio and natural frequency are described as.

$$\zeta = \frac{c}{2 \cdot \sqrt{km}}, \omega_0 = \sqrt{\frac{k}{m}}$$

The force exerted on the beam by the resonators is of opposite direction and is included as a negative forcing term. The kronecker-delta function is used to express the individual point forces. The beam equation with added resonators is then.

$$-\frac{\partial^2 M}{\partial x^2} + c_s I \frac{\partial^5 w_{rel}}{\partial x^4 \partial t^1} + c_e \frac{\partial w_{rel}}{\partial t} + m \frac{\partial^2 w_{rel}}{\partial t^2} = -m \frac{\partial^2 w_b}{\partial t^2} - \sum_{j=1}^S m_j \left(\ddot{u}_j + \frac{\partial^2}{\partial t^2} w_{rel}(x_j, t) + \dot{w}_b \right) \cdot \delta(x - x_j) + f_{ext}(x, t)$$

5.3. Bending Stress in the Piezo Elements

To express the electrical coupling between the piezo elements and the mechanics of the beam the bending moment is expressed. Only the voltage generated because of normal forces are considered in the derivation. The bending moment is a sum of all normal force times their leverage. The total bending force is a combination of the piezopatches and the substrate of the beam. The patches are placed symmetrically on both sides of the beam.

$$M(x, t) = \int_A \sigma_N z \, dA = b \int_{-\frac{h_s}{s} - \frac{h_p}{p}}^{-\frac{h_s}{s}} \sigma_N z \, dz + b \int_{-\frac{h_s}{s}}^{\frac{h_s}{s}} \sigma_N z \, dz + b \int_{\frac{h_s}{s}}^{\frac{h_s}{s} + \frac{h_p}{p}} \sigma_N z \, dz$$

Where M is the bending moment, σ_N is the normal stress in the x -direction, b is the uniform width of the beam, h_s is the thickness of the substrate and s_p is the thickness of the piezo patch. The stress, strain and electric field in the piezo-material has the following relation

$$T_1 = \overline{c}_{11} S_1 - \overline{e}_{13} E_3$$

where T_1 is the normal stress, \overline{c}_{11} is the component of the stiffness tensor that connects normal stress and strain, S_1 is the normal strain, \overline{e}_{13} is the piezo-electric constant that relates the normal stress to an orthogonal electric field. The expression is inserted in the integrals.

$$M(x, t) = b \int_{-\frac{h_s}{s} - \frac{h_p}{p}}^{-\frac{h_s}{s}} (\overline{c}_{11} S_1 - \overline{e}_{13} E_3) z \, dz + b \int_{-\frac{h_s}{s}}^{\frac{h_s}{s}} (Y_s S_1) z \, dz + b \int_{\frac{h_s}{s}}^{\frac{h_s}{s} + \frac{h_p}{p}} (\overline{c}_{11} S_1 - \overline{e}_{13} E_3) z \, dz$$

The electric field is voltage per thickness of the Piezo. For a series connection the potential is a sum of the individual potentials. This relates the electric field to voltage. The strain given by the second derivative of the deflection and negative in compression.

$$E_3 = \frac{V_s}{2h_p}, S_1 = -z \frac{\partial^2 w}{\partial x^2}$$

Where, V_s is the total potential over the two piezo elements connected in series. Inserting these equations and solving yields expressions for the bending moment in the piezo connected in series.

$$M_s(x, t) = -YI \cdot \frac{\partial^2 w_{rel}}{\partial x^2} + \theta_s V_s \{H(x) - H(x - L)\}$$

Where a geometrical and piezo constant and the effective bending stiffness is defined.

$$\theta_s = \frac{\overline{e}_{31} b}{2 h_p} \left[\left(h_p + \frac{h_s}{2} \right)^2 - \left(\frac{h_s}{4} \right)^4 \right], YI = \frac{2 b}{3} \left[\frac{Y_s h_s^3}{8} + \overline{c}_{11} \left(h_p + \frac{h_s}{2} \right)^3 - \frac{h_s^3}{8} \right]$$

The piezo elements for this project have been connected in series. The expression for the bending moment can be inserted in the beam equation, but needs to be derived twice with respect to x . The heavyside function derived once is the kronecker-delta function.

$$\frac{\partial^2 M}{\partial x^2} = -YI \cdot \frac{\partial^4 w_{rel}}{\partial x^4} + \theta_s V_s \left\{ \frac{\partial \delta(x)}{\partial x} - \frac{\partial \delta(x - L)}{\partial x} \right\}$$

⇒

$$YI \cdot \frac{\partial^4 w_{rel}}{\partial x^4} + \theta_s V_s \left\{ \frac{\partial \delta(x)}{\partial x} - \frac{\partial \delta(x-L)}{\partial x} \right\} + c_s I \frac{\partial^5 w_{rel}}{\partial x^4 \partial t^1} + c_e \frac{\partial w_{rel}}{\partial t} + m \frac{\partial^2 w_{rel}}{\partial t^2} = \\ -m \frac{\partial^2 w_b}{\partial t^2} - \sum_{j=1}^S m_j \left(\ddot{u}_j + \frac{\partial^2}{\partial t^2} w_{rel}(x_j, t) + \ddot{w}_b \right) \cdot \delta(x - x_j) + f_{ext}(x, t)$$

5.4. Piezo Electric Potential Equation

The equation governing the potential created by the piezo electric elements is derived in this section. The direct piezoelectric effect connects the dielectric displacement (Braghin, 2019).

$$D_3 = e_{31} S_1 + \epsilon_{33} E_3$$

Where S_1 is normal strain, D_3 is dielectric displacement in the z-direction, ϵ_{33} is the permittivity and e_{31} is the piezo electric constant. The dielectric displacement is charge per area.

$$\frac{\partial D_3}{\partial t} A = \frac{\partial Q}{\partial t} \frac{A}{A} = I$$

Where A is the area of piezo electric element. From Ohms' law I is isolated and expressed with the dielectric displacement.

$$-\frac{\partial}{\partial t} \int D \cdot n \, dA = \frac{V}{R_l}$$

The expression for the direct piezoelectric effect is inserted

$$-\frac{\partial}{\partial t} \int_A e_{31} S_1 n + \epsilon_{33} E_3 \cdot n \, dA = \frac{V}{R_l}$$

The stress in the piezo is considered constant over a given cross section. The normal strain is evaluated in the center of the piezo material.

$$\sigma_N = \sigma_{M-y} = \frac{M \cdot y}{I} = S_1 \cdot E \Leftrightarrow S_1 = \frac{My}{I \cdot E}$$

$$M = EI \frac{\partial^2 w_{Rel}}{\partial x^2} \Rightarrow S_1 = \frac{\partial^2 w_{Rel}}{\partial x^2} \cdot \frac{\left(\frac{h_b}{2} + \frac{h_p}{2} \right) \cdot I \cdot E}{I \cdot E} = \frac{\partial^2 w_{Rel}}{\partial x^2} \cdot \left(\frac{h_b}{2} + \frac{h_p}{2} \right)$$

This is inserted and the electric field is expressed as voltage over the thickness of the element.

$$\frac{V}{R_l} + \int_A e_{31} \frac{\partial^3 w_{Rel}}{\partial x^2 \partial t} \cdot \left(\frac{h_b}{2} + \frac{h_p}{2} \right) \cdot n \cdot dA + \varepsilon_{33} \frac{\dot{V}}{h} \cdot bl = 0$$

Integrating over the constant width of the beam gives.

$$\frac{V}{R_l} + e_{31} h_{pc} b \int_0^L \frac{\partial^3 w_{Rel}}{\partial x^2 \partial t} dx + \varepsilon_{33} \frac{\dot{V}}{h} \cdot bl = 0, \quad h_{pc} = \left(\frac{h_b}{2} + \frac{h_p}{2} \right)$$

The relative deflection is expressed with separation of variables. A new placeholder independent of time; K_r is introduced. Using the BC that there is no angular deflection at 0, it can be calculated as follows.

$$w_{rel} = \sum_{r=1}^N \phi_r \eta_r$$

$$K_r = e_{31} h_{pc} b \int_0^L \frac{\partial^2 \phi_r}{\partial x^2} dx = e_{31} h_{pc} b \left(\frac{\partial \phi_r}{\partial x} \Big|_{x=L} - \frac{\partial \phi_r}{\partial x} \Big|_{x=0} \right) = e_{31} h_{pc} b \frac{\partial \phi_r}{\partial x} \Big|_{x=L}$$

$$\frac{V}{R_l} + \sum_{r=1}^N K_r \eta_r + \varepsilon_{33} \frac{\dot{V}}{h} \cdot bl = 0$$

Another two placeholders are introduced to simplify the equation.

$$i_p = \sum_{r=1}^N K_r \eta_r, \quad c_p = \varepsilon_{33} \frac{bl}{h}$$

$$\Rightarrow$$

$$\frac{V(t)}{R_l} + i_p(t) + c_p \dot{V}(t) = 0$$

5.5. Further Derivation of the Beam Equation

The relative displacements are discretized using separation of variables as shown previously.

$$w_{rel} = \sum_{r=1}^N \phi_r(x) \eta_r(t)$$

The equation is multiplied with $\phi_s(x)$. The dependence on x and t is omitted.

$$\sum_{r=1}^N \phi_s YI \cdot \frac{\partial^4 \phi_r}{\partial x^4} \eta_r + \phi_s \theta_s V_s \left\{ \frac{\partial \delta(x)}{\partial x} - \frac{\partial \delta(x-L)}{\partial x} \right\} + \sum_{r=1}^N \phi_s c_s \frac{\partial^5 \phi_r}{\partial x^4 \partial t^1} \eta_r + \sum_{r=1}^N \phi_s c_e \frac{\partial \phi_r}{\partial t} \eta_r + \sum_{r=1}^N \phi_s m \frac{\partial^2 \phi_r}{\partial t^2} \eta_r =$$

$$-\phi_s m \frac{\partial^2 w_b}{\partial t^2} - \sum_{r=1}^N \sum_{j=1}^S \phi_s m_j \frac{\partial^2 \eta_r}{\partial t^2} \phi_r \cdot \delta(x - x_j) - \sum_{j=1}^S \phi_s \ddot{u}_j m_j \cdot \delta(x - x_j) - \sum_{j=1}^S \phi_s \dot{w}_b m_j \cdot \delta(x - x_j) + \phi_s f_{ext}(x, t)$$

Since the mode-shapes are orthogonal and the previously derived mode-shapes are normalized with respect to the root of the mass the following conditions holds.

$$\int_0^L \phi_s \phi_r m dx = \delta_{sr}$$

$$\int_0^L \phi_s YI \frac{\partial^4 \phi_r}{\partial x^4} dx = \frac{\lambda_r^4 YI}{m L^4} \delta_{sr} = \omega_r^2 \delta_{sr}, \quad \omega_r = \lambda_r^2 \sqrt{\frac{YI}{m L^4}}$$

These conditions are used by integrating over the length of the beam. Some terms have fractions introduced to meet the orthogonality conditions.

$$\int_0^L \left(\sum_{r=1}^N \phi_s YI \frac{\partial^4 \phi_r}{\partial x^4} \eta_r + \phi_s \theta_s V_s \left\{ \frac{\partial \delta(x)}{\partial x} - \frac{\partial \delta(x-L)}{\partial x} \right\} + \sum_{r=1}^N \phi_s \frac{YI}{m L^4} \frac{\partial^4 \phi_r}{\partial x^4} c_s I \frac{\partial \eta_r}{\partial t} + \sum_{r=1}^N \phi_s \frac{m}{m} \phi_r c_e \frac{\partial \eta_r}{\partial t} + \sum_{r=1}^N \phi_s m \phi_r \frac{\partial^2 \eta_r}{\partial t^2} = \right. \\ \left. - \phi_s m \frac{\partial^2 w_b}{\partial t^2} - \sum_{r=1}^N \sum_{j=1}^S \phi_s m_j \frac{\partial^2 \eta_r}{\partial t^2} \phi_r \cdot \delta(x - x_j) - \sum_{j=1}^S \phi_s \ddot{u}_j m_j \cdot \delta(x - x_j) - \sum_{j=1}^S \phi_s \dot{w}_b m_j \cdot \delta(x - x_j) + \phi_s f_{ext}(x, t) \right) dx$$

The following property of the kronegger-delta function is applied for the resonator terms

$$\int_0^L \delta(x - x_j) \phi_s dx = \phi_s(x_j)$$

$$\sum_{r=1}^N \omega_r^2 \delta_{sr} \eta_r + \int_0^L \phi_s \theta_s V_s \left\{ \frac{\partial \delta(x)}{\partial x} - \frac{\partial \delta(x-L)}{\partial x} \right\} dx + \sum_{r=1}^N \omega_r^2 \delta_{sr} \frac{c_s I}{YI} \frac{\partial \eta_r}{\partial t} + \sum_{r=1}^N \frac{\delta_{sr}}{m} \frac{\partial \eta_r}{\partial t} c_e + \sum_{r=1}^N \frac{\partial^2 \eta_r}{\partial t^2} \delta_{sr} = \\ - \dot{w}_b \int_0^L \phi_s m dx - \sum_{r=1}^N \sum_{j=1}^S \phi_s(x_j) \phi_r(x_j) m_j \frac{\partial^2 \eta_r}{\partial t^2} - \sum_{j=1}^S \phi_s(x_j) \dot{u}_j m_j - \dot{w}_b \sum_{j=1}^S \phi_s(x_j) m_j + \int_0^L \phi_s f_{ext}(x, t) dx$$

All the sum terms with the kronegger-delta function are simplified as only one part of them will be non-zero.

$$\omega_s^2 \eta_s + \int_0^L \phi_s \theta_s V_s \left\{ \frac{\partial \delta(x)}{\partial x} - \frac{\partial \delta(x-L)}{\partial x} \right\} dx + \omega_s^2 \frac{c_s I}{YI} \dot{\eta}_s + \frac{c_e}{m} \eta_s + \ddot{\eta}_s =$$

$$-\ddot{w}_b \left(\sum_{j=1}^S \phi_s(x_j) m_j + m \int_0^L \phi_s dx \right) - \sum_{r=1}^N \sum_{j=1}^S \phi_s(x_j) \phi_r(x_j) m_j \ddot{\eta}_r - \sum_{j=1}^S \phi_s(x_j) i j m_j + \int_0^L \phi_s f_{ext}(x, t) dx$$

Similarly to the resonator terms integration over the kronegger-delta function is performed and a placeholder is introduced.

$$\int_0^L \phi_s \theta_s V_s \left\{ \frac{\partial \delta(x)}{\partial x} - \frac{\partial \delta(x-L)}{\partial x} \right\} dx = \theta_s V_s \frac{\partial \phi_s(x)}{\partial x} \Big|_{x=0} - \theta_s V_s \frac{\partial \phi_s(x)}{\partial x} \Big|_{x=L} = - \frac{\partial \phi_s(x)}{\partial x} \Big|_{x=L} \theta_s V_s = -\chi_s V_s$$

All terms are divided with the mass of the beam mL. The relative mass \hat{m} of a resonator to the beam is introduced. The damping terms are unified by defining a damping pooled damping ratio.

$$\hat{m}_j = \frac{m_j}{m \cdot L}, \quad 2 \zeta_s \omega_s = \frac{c_s I \cdot \omega_s^2}{YI} + \frac{c_e}{m}$$

Inserting the expressions gives.

$$\frac{\omega_s^2 \eta_s}{mL} - \frac{\chi_s}{mL} V_s + \frac{1}{mL} 2 \zeta_s \omega_s \dot{\eta}_s + \frac{\ddot{\eta}_s}{mL} =$$

$$-\ddot{w}_b \left(\sum_{j=1}^S \phi_s(x_j) \hat{m}_j + \frac{1}{L} \int_0^L \phi_s dx \right) - \sum_{r=1}^N \sum_{j=1}^S \phi_s(x_j) \phi_r(x_j) \hat{m}_j \ddot{\eta}_r - \sum_{j=1}^S \phi_s(x_j) i j \hat{m}_j + \int_0^L \phi_s f_{ext}(x, t) dx$$

5.6. Assuming Harmonic Solutions

The transient response of the variables is neglected and therefore it can be assumed that η , V and u are harmonic with the same frequency as the base motion. (Inman, Piezoelectric Energy Harvesting - Appendix C Modal Analysis of a Uniform Cantilever with a Tip Mass, 2011).

$$\eta_s = H_{s0} e^{j\omega t}, \quad u_j = U_{j0} e^{j\omega t}, \quad V = V_0 e^{j\omega t}, \quad w_b = w_{b0} e^{j\omega t}$$

As all terms includes the same exponential only the constants are included. Using simple derivations with time, the beam equation 1), resonator equation 2) and the piezo equation 3) are now expressed as:

1)

$$\frac{\omega_s^2}{mL} H_{s0} - \frac{\chi_s}{mL} V_{s0} + \frac{1}{mL} 2j \zeta_s \omega_s \omega H_{s0} - \frac{\omega^2 H_{s0}}{mL} =$$

$$\omega^2 w_{b0} \left(\sum_{j=1}^S \phi_s(x_j) \hat{m}_j + \frac{1}{L} \int_0^L \phi_s dx \right) + \sum_{r=1}^N \sum_{j=1}^S \phi_s(x_j) \phi_r(x_j) \hat{m}_j \omega^2 H_{r0} + \sum_{j=1}^S \phi_s(x_j) \hat{m}_j \omega^2 U_{j0} + \int_0^L \phi_s f_{ext}(x, t) dx$$

2)

$$-\omega^2 U_{j0} + 2j\zeta\omega_0\omega U_{j0} + \omega_0^2 U_{j0} - \sum_{r=1}^N \omega^2 \phi_r(x_j) H_{r0} = \omega^2 w_{b0} \Leftrightarrow U_{j0} = \frac{\omega^2 w_{b0} + \sum_{r=1}^N \omega^2 \phi_r(x_j) H_{r0}}{\omega_0^2 - \omega^2 + 2j\zeta\omega_0\omega}$$

3)

$$\frac{V_0}{R_l} + j\omega \sum_{r=1}^N K_r H_{r0} + jC_p V_0 = 0$$

Inserting 2 in 1.

$$\frac{1}{mL} (\omega_s^2 - \omega^2) H_{s0} - \frac{\chi_s}{mL} \cdot V_0 + \frac{1}{mL} 2j \zeta_s \omega_s \omega H_{s0} =$$

$$\omega^2 w_{b0} \left(\sum_{j=1}^S \phi_s(x_j) \hat{m}_j + \frac{1}{L} \int_0^L \phi_s dx \right) + \sum_{r=1}^N \sum_{j=1}^S \phi_s(x_j) \phi_r(x_j) \hat{m}_j \omega^2 H_{r0} + \sum_{j=1}^S \phi_s(x_j) \hat{m}_j \omega^2 \frac{\omega^2 w_{b0} + \sum_{r=1}^N \omega^2 \phi_r(x_j) H_{r0}}{\omega_0^2 - \omega^2 + 2j\zeta\omega_0\omega} + \int_0^L \phi_s f_{ext}(x, t) dx$$

By extending the fraction in the two resonator terms a simplification can be made.

$$\frac{1}{mL} (\omega_s^2 - \omega^2) H_{s0} - \frac{\chi_s}{mL} \cdot V_0 + \frac{1}{mL} 2j \zeta_s \omega_s \omega H_{s0} - \omega^2 \sum_{j=1}^S \phi_s(x_j) \hat{m}_j \frac{\omega^2 w_{b0}}{\omega_0^2 - \omega^2 + 2j\zeta\omega_0\omega}$$

$$- \frac{\omega_0^2 + 2j\zeta\omega_0\omega}{\omega_0^2 - \omega^2 + 2j\zeta\omega_0\omega} \omega^2 \sum_{r=1}^N \sum_{j=1}^S \phi_s(x_j) \phi_r(x_j) \hat{m}_j H_{r0} = \omega^2 w_{b0} \sum_{j=1}^S \phi_s(x_j) \hat{m}_j + \frac{\omega^2 w_{b0}}{L} \int_0^L \phi_s dx + \int_0^L \phi_s f_{ext}(x, t) dx$$

A similar operation is made with fourth and sixth' term of the equation.

$$\begin{aligned} \frac{1}{mL} (\omega_s^2 - \omega^2) H_{s0} - \frac{\chi_s}{mL} \cdot V_0 + \frac{1}{mL} 2j\zeta_s \omega_s \omega H_{s0} - \frac{(\omega_0^2 + 2j\zeta\omega_0\omega)\omega^2}{\omega_0^2 - \omega^2 + 2j\zeta\omega_0\omega} w_{b0} \sum_{j=1}^S \phi_s(x_j) \hat{m}_j = \\ - \frac{(\omega_0^2 + 2j\zeta\omega_0\omega)\omega^2}{\omega_0^2 - \omega^2 + 2j\zeta\omega_0\omega} \sum_{r=1}^N \sum_{j=1}^S \phi_s(x_j) \phi_r(x_j) \hat{m}_j H_{r0} - \frac{\omega^2 w_{b0}}{L} \int_0^L \phi_s dx + \int_0^L \phi_s f_{ext}(x, t) dx \end{aligned}$$

A placeholder is introduced that is constant for a given excitation frequency.

$$\begin{aligned} C &= \frac{(\omega_0^2 + 2j\zeta\omega_0\omega)\omega^2}{\omega_0^2 - \omega^2 + 2j\zeta\omega_0\omega} \\ &\Rightarrow \\ \frac{1}{mL} (\omega_s^2 - \omega^2) H_{s0} - \frac{\chi_s}{mL} \cdot V_0 + \frac{1}{mL} 2j\zeta_s \omega_s \omega H_{s0} - C w_{b0} \sum_{j=1}^S \phi_s(x_j) \hat{m}_j - C \sum_{r=1}^N \sum_{j=1}^S \phi_s(x_j) \phi_r(x_j) \hat{m}_j H_{r0} &= \\ - \frac{\omega^2 w_{b0}}{L} \int_0^L \phi_s dx + \int_0^L \phi_s f_{ext}(x, t) & \end{aligned}$$

This equation can be isolated in matrix form for H_{s0} expressed with V_0 . Damping and external force is neglected. The two terms containing the base motion and are defined as vectors with entries as:

$$Q_{2,s} = \frac{\omega^2 w_{b0}}{L} \int_0^L \phi_s dx, \quad Q_{1,s} = C w_{b0} \sum_{j=1}^S \phi_s(x_j) \hat{m}_j$$

The beam equation is now expressed as.

$$\frac{1}{mL} (\omega_s^2 - \omega^2) H_{s0} - \frac{\chi_s}{mL} \cdot V_0 - C \sum_{r=1}^N \sum_{j=1}^S \phi_s(x_j) \phi_r(x_j) \hat{m}_j H_{r0} = Q_{2,s} + Q_{1,s}$$

This can be put in matrix form

$$(\Omega - \Phi) H = Q_2 + Q_1 + X \cdot V_0$$

$$\Omega = \frac{1}{mL} \begin{bmatrix} \omega_1^2 - \omega^2 & 0 & 0 \\ 0 & \omega_2^2 - \omega^2 & 0 \\ 0 & 0 & \omega_n^2 - \omega^2 \end{bmatrix}, \quad H = \begin{bmatrix} H_{10} \\ H_{20} \\ H_{n0} \end{bmatrix}$$

$$\Phi = C \sum_{j=1}^S \hat{m}_j \begin{bmatrix} \phi_1(x_j)\phi_1(x_j) & \phi_1(x_j)\phi_2(x_j) & \phi_1(x_j)\phi_n(x_j) \\ \phi_2(x_j)\phi_1(x_j) & \phi_2(x_j)\phi_2(x_j) & \phi_2(x_j)\phi_n(x_j) \\ \phi_n(x_j)\phi_1(x_j) & \phi_n(x_j)\phi_2(x_j) & \phi_n(x_j)\phi_n(x_j) \end{bmatrix}, \quad X = \frac{1}{mL} \begin{bmatrix} \chi_1 \\ \chi_2 \\ \vdots \\ \chi_n \end{bmatrix}$$

Where matrices are of dimension (n x n) where n is the number of mode-shapes included in the calculation. Isolating for H yields.

↔

$$H = (\Omega - \Phi)^{-1} (Q_2 + Q_1 + X \cdot V_0)$$

The derived voltage equation can be expressed as a scalar equation with matrices.

$$KH + \left(jc_p + \frac{1}{R_l} \right) V_0 = 0$$

Where

$$K = j\omega \begin{bmatrix} K_1 & K_2 & K_n \end{bmatrix}$$

The expression for H is inserted and the equation is solved for the voltage.

$$\Rightarrow K(\Omega - \Phi)^{-1} (Q_2 + Q_1 + X \cdot V_0) + \left(jc_p + \frac{1}{R_l} \right) V_0 = 0$$

↔

$$V_0 = - \frac{K(\Omega - \Phi)^{-1} (Q_2 + Q_1)}{K(\Omega - \Phi)^{-1} X + jc_p + \frac{1}{R_l}}$$

Here it's important to notice that all individual terms are scalars. After calculating the voltage, the tip deflection can be found from previous equation. This yields resonator vibration amplitude.

$$H = (\Omega - \Phi)^{-1} (Q_2 + Q_1 + X \cdot V_0)$$

The resonator amplitudes are given by

$$U = Q_3 + \Phi_2 H,$$

Where

$$\Phi_2 = \frac{\omega^2}{\omega_0^2 - \omega^2 + 2j\zeta\omega_0\omega} \begin{bmatrix} \phi_1(x_1) & \phi_2(x_1) & \phi_n(x_1) \\ \phi_1(x_2) & \phi_2(x_2) & \phi_n(x_2) \\ \phi_1(x_3) & \phi_2(x_3) & \phi_n(x_3) \end{bmatrix}, \quad U = \begin{bmatrix} U_{10} \\ U_{20} \\ U_{n0} \end{bmatrix}, \quad Q_3 = \frac{\omega^2 w_{b0}}{\omega_0^2 - \omega^2 + 2j\zeta\omega_0\omega} \begin{bmatrix} 1 \\ 1 \\ 1 \end{bmatrix}$$

6. Numerical simulation of beam

Using the expressions for the beam deflection, resonator movement and piezoelectric coupling derived in the previous section, numerical simulations can be carried out of the beam, subject to different parameters in order to define their influences and possible optimal conditions for bandgap formation and energy harvesting.

To the steel beam, a compound damping coefficient of $\xi = 0.001$ is assigned, an arbitrary low value that could be selected based on experiments. This low damping value allows to better study the resonance effects that will occur in the cantilever beam. For the other parameters that need to be specified, an initial assumption is made, based on which the optimisation of these parameters will be carried out. To keep the added mass low, the total resonator mass is set to 20 % of the beam mass. The chosen piezoelectric material is PZT-5A. Finally, a negligible value for the resonator damping is chosen, in order to optimally see the effects of the spring-masses. The initial assumed values are listed in table 2 (Charles Sherman, 2007).

Mass ratio	0,2	\bar{e}_{31} [C/m ²]	-10.4
M _j [kg]	0,0025	$\bar{\epsilon}_{33}$ [F/m]	13.3 E-9
N – resonator count	10	\bar{c}_{11} [GPa]	61
K _j [N/m]	3.07 E4	ρ_p [kg/m ³]	7750
ξ [/]	≈ 0	R _L [ohm]	1000
		H _p [m]	0.15 E-3

TABLE 2: INITIALLY GUESSED PARAMETERS

The damper spring and mass are chosen in such a way that their resonance frequency falls on the fifth resonance frequency of the beam, which was found to be at 3505 rad/s or 558Hz.

Using this initial data, the previously derived formulas can be used to create FRF of the absolute tip displacement, which can in turn be compared to the FRF of a simple cantilever beam with the same properties, but without resonators or piezoelectric patches. These FRF's are displayed in figures 4 and 5.

The dotted vertical lines represent the bandwidth as predicted by the resonator data: $\omega_t = \sqrt{\frac{k_j}{m_j}}$ and $BW = \omega_t \cdot (1 - \sqrt{1 + \mu})$, $\mu = \frac{\sum_{j=1}^N m_j}{m_{struct}}$ (Christopher Sugino, 2016). As can been seen in figure 5, the simulation follows this prediction closely. For these calculations, the first 10 modeshapes have been considered. As can been seen by comparing both figures, the interaction of the beam with the resonators heavily influences its behavior in the frequency spectrum, introducing many amplitude peaks where the resonators go into resonance. A bandgap has been introduced around the frequency of the fifth modeshape of the normal cantilever beam.

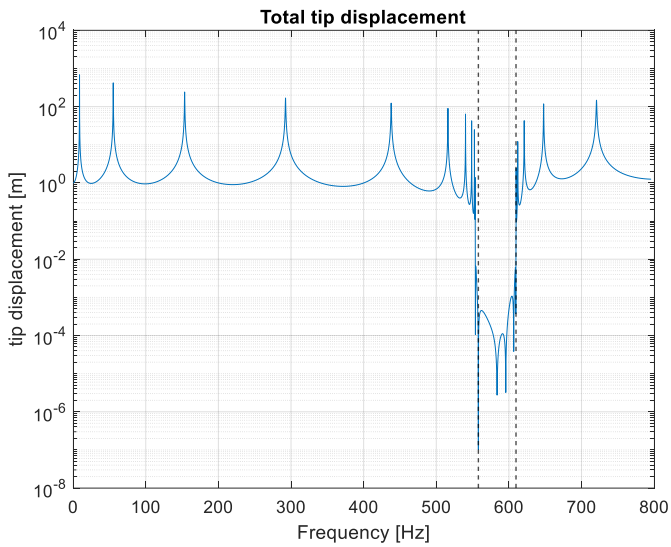


FIGURE 4: TOTAL TIP DISPLACEMENT

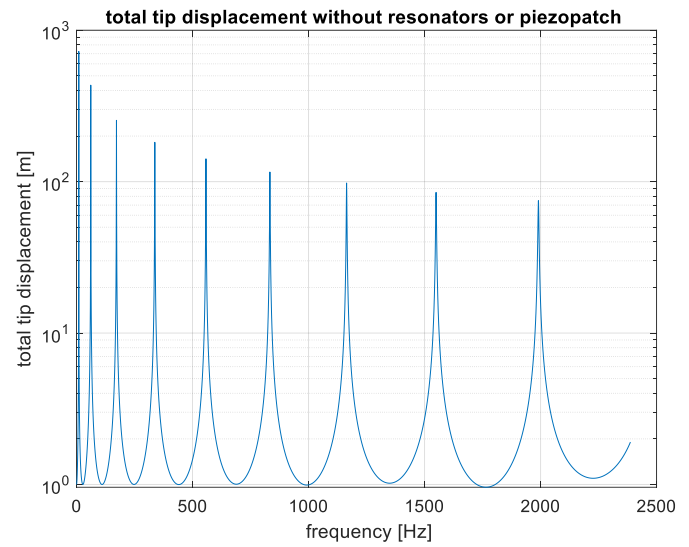


FIGURE 5: TOTAL TIP DISPLACEMENT OF SIMPLE CANTILEVER BEAM

In figure 6, the amplitude of all resonators, relative to the motion of the beam, has been displayed, along with the relative beam movement at the positions of the resonators.

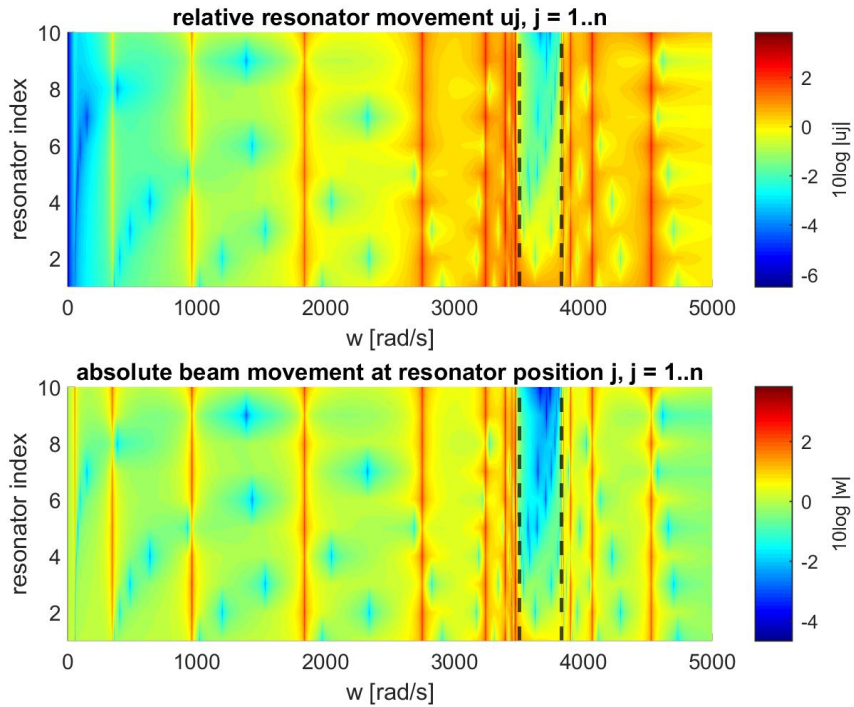


FIGURE 6: RESONATOR AND BEAM DEFLECTIONS

From these figures, it is evident that the resonators go into resonance together with the resonance frequencies of the beam. As the resonators get closer to the tip of the beam (resonator index increases),

their relative amplitude noticeably decreases in the region of the bandgap, indicated by the dotted vertical lines. The resonator amplitude plot also exhibits some discrete frequencies where the relative amplitude goes to zero. The frequencies correspond to the antiresonances on figure displaying the absolute amplitudes of the beam. These antiresonances arise when the contributions of the different modeshape cancel each other out at certain points. Evidently, at these points, there is very little absolute motion of the beam, resulting in the resonator amplitude being very low as well.

Next, through the derivations made earlier, the generated power can be calculated for the different frequencies, and compared to the FRF of the tip deflection. The generated power is displayed in figure 8.

From the comparison, it is evident that the peaks in harvested power closely follow the resonance peaks in the total tip displacement. This is because at those peaks, the beam deflection will be very large, causing a big stress on the piezoelectric patches.

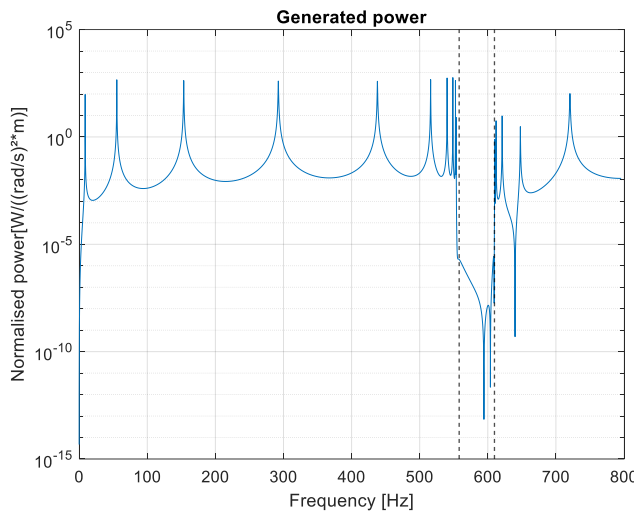


FIGURE 8: GENERATED POWER

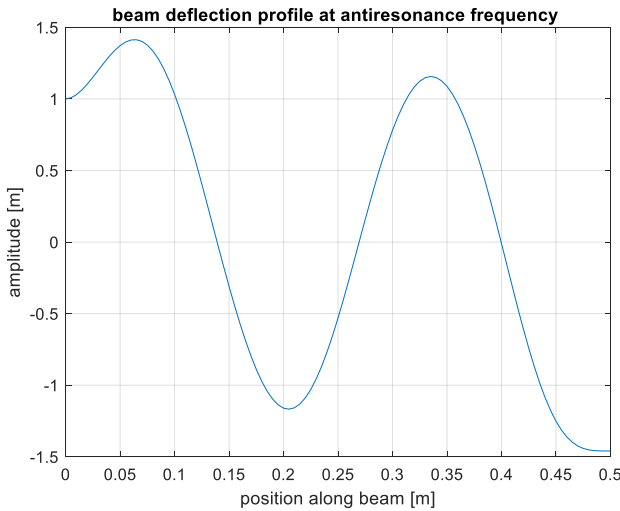


FIGURE 7 ABSOLUTE BEAM DEFLECTION AT ANTIRESONANCE FREQUENCY

segmentation of the piezopatches will be needed. As the mode number goes up, however, the

One remarkable effect can be seen on the power plot around the frequency of 640 Hz. At this point, the power generated by the piezopatches appears to be going to zero, while the total tip deflection does not show any noticeable drops in amplitude. In fact, when looking at a graph of the deflection amplitude along the beam, portrayed in figure 7, the deflection does not appear to be especially low. The sudden drop in generated power can be explained by the contributions to the power of different sections cancelling each other out. If, for example, the beam curves positively in the first half of its length, the piezoelectric patch on the top section will be stretched out. If, simultaneously, the second section of the beam undergoes negative curvature, the piezoelectric patch on the top section will experience a local compression. As a consequence of this varying curvature, the charge separation and subsequent generated electric field will be of opposite sign in the different sections, therefore cancelling each other out. It is conceivable that, if a patch of full length, with only a single electrode is placed on top of a cantilever beam, a significant fraction of the power that could be generated will be lost due to cancellation. This could partially solved by breaking down the patch into separate segments, each connected to its own load, and therefore becoming its own circuit. This way, for at least the first modeshapes, which vary their amplitude along the beam relatively slowly, the contributions to the generated power will not cancel each other out as much. If it were desirable to also harvest a larger fraction of the maximum attainable power in the higher order modeshapes, a larger

contributions of the modeshapes become gradually less due to a decreasing contribution to the total beam deflection. It is therefore sufficient to effectively harvest the energy from the lower order modeshapes.

7. Study of beam parameters

After describing the basic behavior of the cantilever, and its response to the addition of mechanical resonators and piezoelectric patches, the influence of the beam parameters with regards to bandgap formation and energy harvesting can be described, and optimal values for the parameters can be chosen accordingly.

7.1. Influence of mass ratio

As mentioned earlier, the mass ratio is the ratio between the total amount of mass added by the resonators and the mass of the main vibrating structure. In this case, this structure encompasses the cantilever beam, together with the piezoelectric patches attached to its sides. Expressed as a formula, this

becomes: $\mu = \frac{\sum_{j=1}^N m_j}{(\rho_{beam} + \rho_p)L}$. As stated before, the expression for all frequencies in the bandgap is given by

$\omega_t \leq \omega \leq \sqrt{1 + \mu \cdot \omega_t}$ (Christopher Sugino, 2016). Figure 9 depicts the absolute tip displacement as it varies with frequency and mass ratio, where the total resonator mass is equally distributed over the resonators. The dotted lines represent the boundaries of the bandgap as predicted by the equations.

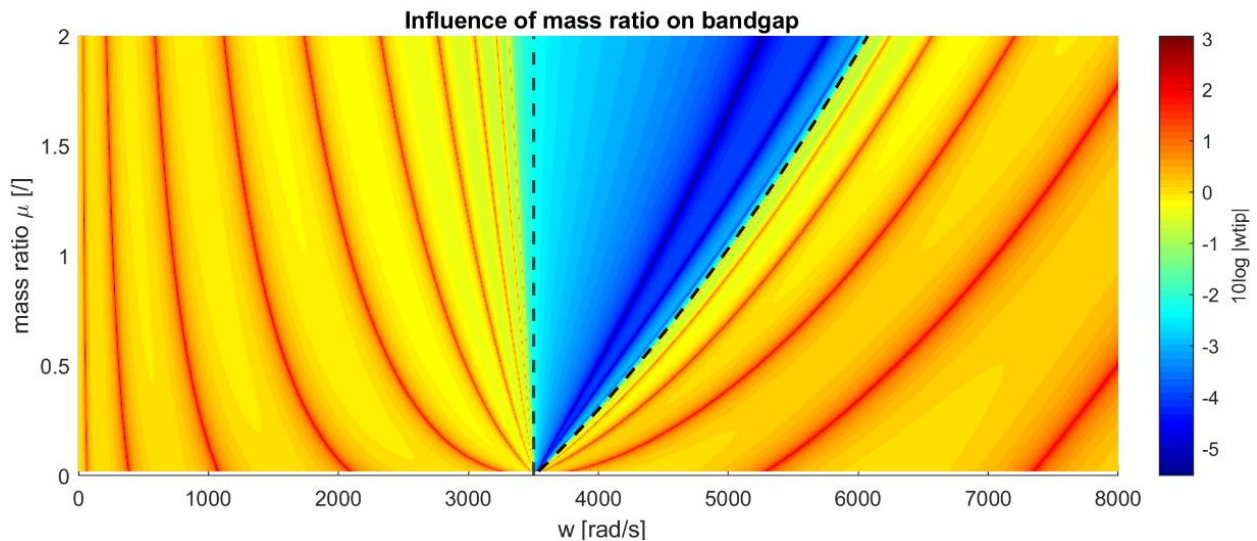


FIGURE 9: INFLUENCE OF MASS RATIO ON BANDGAP

As can be seen in the figure, the results from the simulations follow the predictions from the theory closely. The resonance frequencies of the cantilever beam below the resonance frequency decrease as the mass ratio goes up. This is because increasing the mass decreases the resonance frequency, according

$$\text{to the formula } \omega_{res} = \sqrt{\frac{k_j}{m_j}}$$

Based on this plot, knowing that the width of the bandgap can still be confidently estimated using the known equations, the final, optimal mass ratio can be chosen. Knowing that a bandgap of 50 Hz is desired, a mass ratio of 0.2 is decided upon. Considering the resonance frequencies of the resonators is 558 Hz, this will give a bandgap with a width of 53 Hz.

7.2. Influence of Number of Resonators on Bandgap Formation

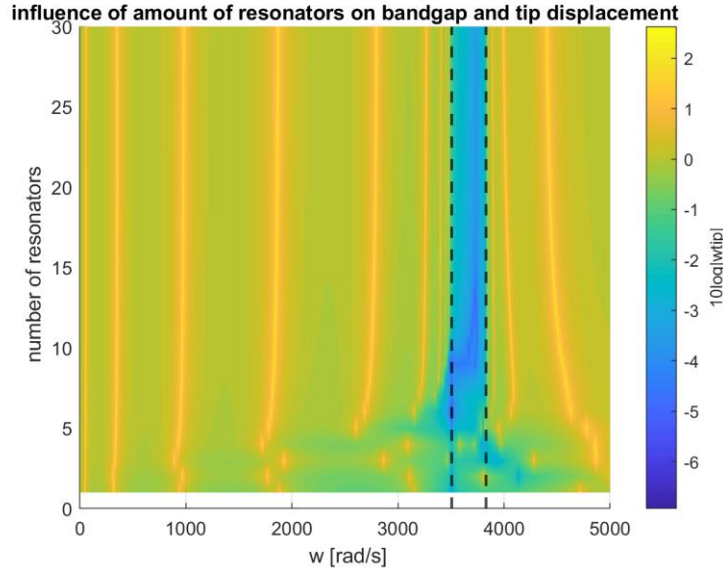


FIGURE 10: EFFECT OF VARYING RESONATOR AMOUNT

To understand the necessary number of resonators to achieve meta-material behavior, beams with 1 to 30 resonators were solved for tip deflection under a sweep of frequencies. Figure 10 displays the result. A smoothing function has been applied to better see the tendency in the otherwise discrete plot. Throughout all the calculations the total mass ratio and the resonance frequency of the resonators are kept constant, so the expected bandgap frequencies are constant. To achieve this, mass and stiffness of the individual resonators are adjusted for each beam.

The result shows that a certain number of resonators are necessary before the behavior of the structure converges and behaves like a meta material. Below five resonators, no bandgap is formed, and resonances even occur within the targeted bandgap area. Ten resonators appear to be enough to achieve convergence to an actual meta-material like behaviour. Therefore, for further simulations the number of 10 resonators is used.

Knowing the amount of resonators used and the desired with and frequencies of the bandgap, the mass and stiffness of the resonators can be derived according to the previously derived formulas.

7.3. Influence of resonator damping ratio

After deciding upon a mass and stiffness for the resonator, the effect of the resonator stiffness can be analysed. Figure 11 displays the influence of the resonator damping on the harvested power and tip displacement. The damping has little influence on the location of the resonance frequencies and the width of the bandgap, as was expected, judging by the fact that the damping term does not appear in the formulas for these parameters. As the damping increases and becomes significantly large, the resonance peaks and bandgap become more and more attenuated. At damping values of order of magnitude of 10^{-1} , the bandgap becomes hard to distinguish from the other parts of the frequency spectrum, because the damping effect is too high. With the eye on bandgap creation, the damping should therefore be chosen significantly low, or even as close to zero as possible.

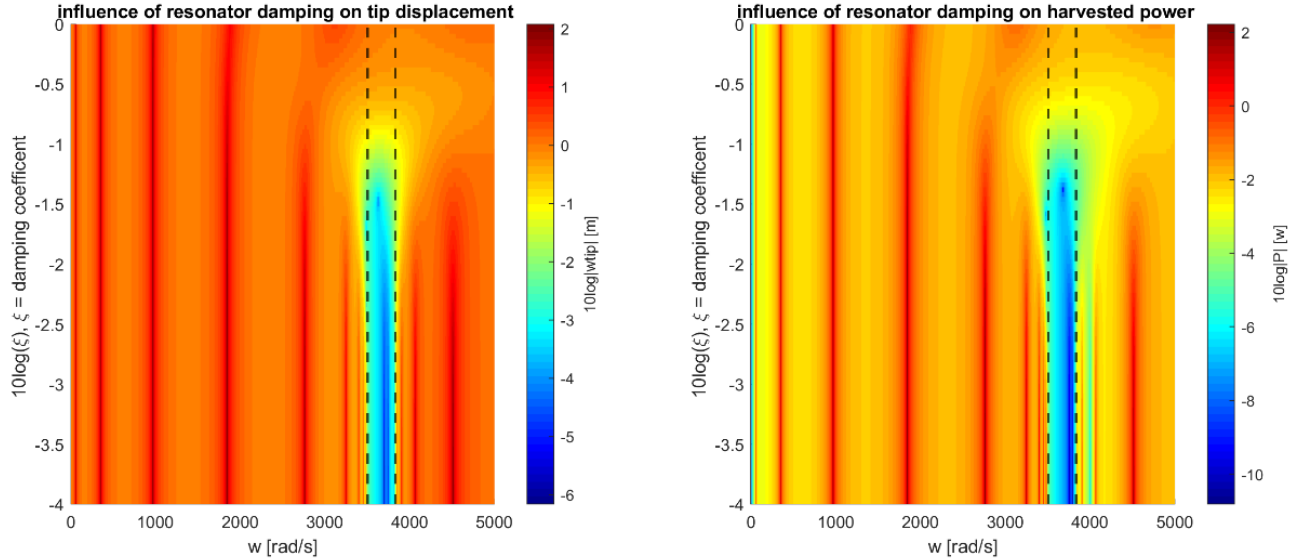


FIGURE 11: INFLUENCE OF RESONATOR DAMPING

Also when assessing the maximum power harvesting, the damping value should be chosen low. This is because the energy harvesting would likely be optimized and executed at resonance frequencies of the beam, in order to make optimal use of the beam vibrations. As damping goes up, the resonance peaks, and therefore the harvestable power, gets attenuated.

One reason why a nonzero value for the damping might be desirable is to prevent mechanical failure. At resonance, the tip displacement could become potentially high enough as to cause mechanical failure in the beam. Those cases can be prevented by choosing an appropriate damping value, which is high enough to prevent failure, but still low enough to allow a good fraction of the energy to be harvested.

In order to be able to see the effect of parameters on the beam to their full extent, for the duration of the report, a negligible value is assigned to the damping. In real life applications, of course, a nonzero value would be chosen.

7.4. Choice of piezoelectric material

When building the piezopatches, a choice of material has to be made. With regards to energy harvesting capabilities, certain materials might perform better than others. For this application, three different materials will be compared, after which a final choice for the material will be made. The materials, which are all commercially available, are PZT-5A, PZT-5H and PMN-PT(33%). Their respective properties are listed in tables 3 to 5.

PZT-5A		PZT-5H		PMN-PT 33%	
\bar{e}_{31} [C/m ²]	-10.4	\bar{e}_{31} [C/m ²]	-16.6	\bar{e}_{31} [C/m ²]	-19
$\bar{\epsilon}_{33}$ [F/m]	13.3 E-9	$\bar{\epsilon}_{33}$ [F/m]	25.55 E-9	$\bar{\epsilon}_{33}$ [F/m]	47.2 E-9
\bar{c}_{11} [GPa]	61	\bar{c}_{11} [GPa]	60.9	\bar{c}_{11} [GPa]	14.26
ρ_p [kg/m ³]	7750	ρ_p [kg/m ³]	7500	ρ_p [kg/m ³]	8083

TABLES 3-5: PIEZOELECTRIC MATERIAL DATA (CHARLES SHERMAN, 2007)

The piezoelectric coupling of PMN-PT 33% is higher than PZT-5H, which is in turn higher than the one of PZT-5A.

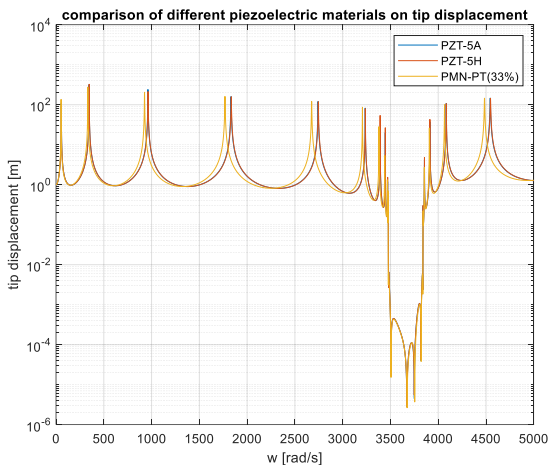


FIGURE 12: DIFFERENT PIEZOELECTRIC MATERIALS ON TIP DISPLACEMENT

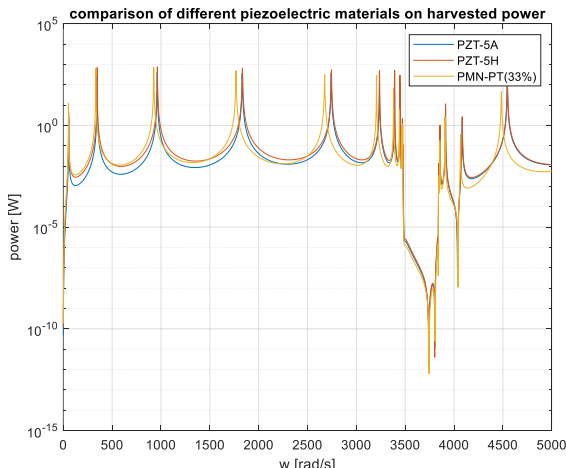


FIGURE 13: DIFFERENT PIEZOELECTRIC MATERIALS ON HARVESTED POWER

Figures 12 and 13 display a comparison between these materials, with regards to the tip displacement and harvested power. Despite the differences in their properties, little difference can be noticed with respect to their effect on the behavior of the structure. They appear to have little effect on the bandgap width, which makes sense, as they could only influence it by their added masses, which are close to each other.

PMN-PT 33% does appear to have an influence on the position of the resonance peaks of the structure. This is likely due to its added mass and greatly reduced stiffness, affecting the total structure stiffness.

In terms of harvesting power, the three materials attain comparable results. In the neighborhood of the bandgap, which is where the energy harvesting will be done, PZT-5H attains slightly better results as the other materials, although this result is very small. Because of this slight advantage, the choice is made to set the piezoelectric material used to PZT-5H

7.5. Thickness of the Piezo Elements

To optimize the harvested power, it's important to consider the thickness of the applied piezo-electric materials. In figure 14 the generated power and the tip deflection have been plotted over a range of frequencies for various piezo thicknesses.

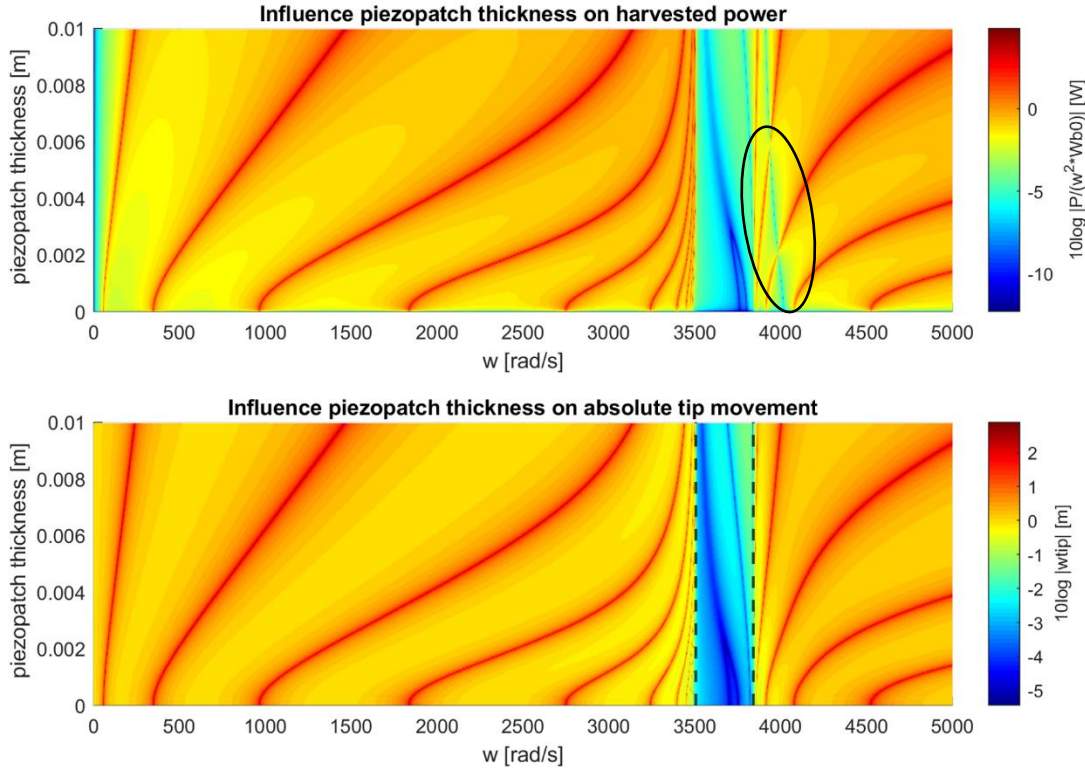


FIGURE 14: INFLUENCE OF PIEZOPATCH THICKNESS

The harvested power is normalized with the frequency squared, which correlates linearly with the energy content of the motion. It is shown that thicker piezo-electric elements generate more voltage as could have been expected. Increasing the thickness of the piezo element makes the structure significantly heavier and the thickness should be limited. Other ways of optimizing the power output are sought. Furthermore, the power generation and the tip displacement have same resonance lines and generally correlate. The resonance lines move towards higher frequencies as the piezo elements get thicker. This is because with increasing piezopatch thickness, the beam gets stiffer, and this increase in stiffness is more dominant than the effect of the added mass.

In one area of the graph, encircled in black, a surprising attenuation line occurs in the power generation. This line is the same mode cancellation line as was found in figure 8, only extended over multiple piezo thicknesses. It is likely that the generated potential is reversed after this line. This stresses the fact that mode cancellation causes a significant power loss.

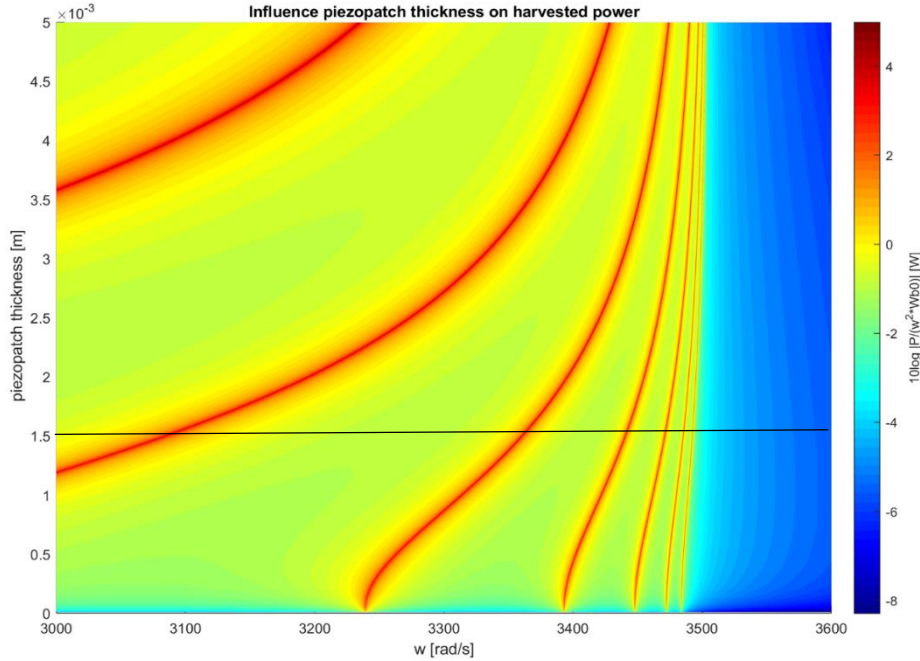


FIGURE 15: VARYING PIEZOPATCH THICKNESS IN THE SPECTRUM OF INTEREST FOR ENERGY HARVESTING

The project group decided to focus on energy harvesting from 3000rad/s until the bandgap to simulate an application where the beam is excited in the frequency range and harvesting is needed, while the beam is not allowed to transfer frequencies in the bandgap. To better understand the area, a closeup of the region is examined in figure 15. It was found that one of the resonance frequencies have an almost horizontal development for increasing piezo element thickness at 1.5mm thickness. Choosing piezo element thickness to be intersecting at this close to horizontal part will yield higher power outputs than a thicker element over an interval of about 200rad/s. This is due to the more widened resonance frequency. Utilizing non-linear properties could spread out these frequencies further and has potential to increase the power output for even more frequencies.

7.6. Influence of load resistance

The electrical load attached to the piezoelectric patch in the electric circuit influences the amount of power that flows through the system, and can therefore be optimized for a specific frequency at which the harvesting can occur. Figure 16 displays the effect of increasing the resistance value on the generated voltage and current in the system, where the current is given by $I = \frac{V}{R_L}$, and the voltage is calculated via the derived equations.

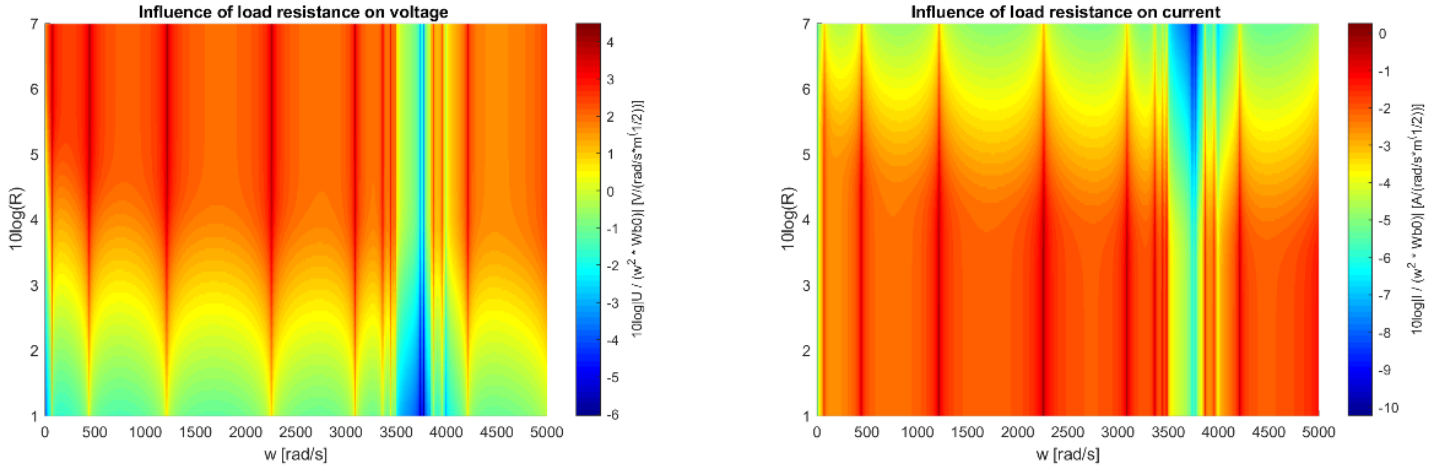


FIGURE 16: INFLUENCE OF VARYING LOAD ON GENERATED VOLTAGE AND CURRENT

As is clear in the graphs, the generated voltage increases with increasing load values. On the other hand, because the resistance is also found in the denominator of the equation, and this term is more dominant than the voltage increase, the current decreases as the resistance increases. When power and current are multiplied to obtain power, due to the opposite tendencies of voltage and current, for a single frequency, a single optimal resistance value will be found.

The harvested power and tip displacement as they vary with frequency and resistance value is displayed in figure 17. Contrarily to the power, the resistance has very little to no influence on the tip displacement. The dotted line traces out the resistance that optimises the power at any frequency. As stated earlier, the goal in this report is to harvest a maximal amount of power in the frequency band of 3000 rad/s until 3500 rad/s. For this frequency band, and for the parameters derived earlier in the report, the optimal value of the resistance is found to be approximately $R_L = 10^4 \Omega$.

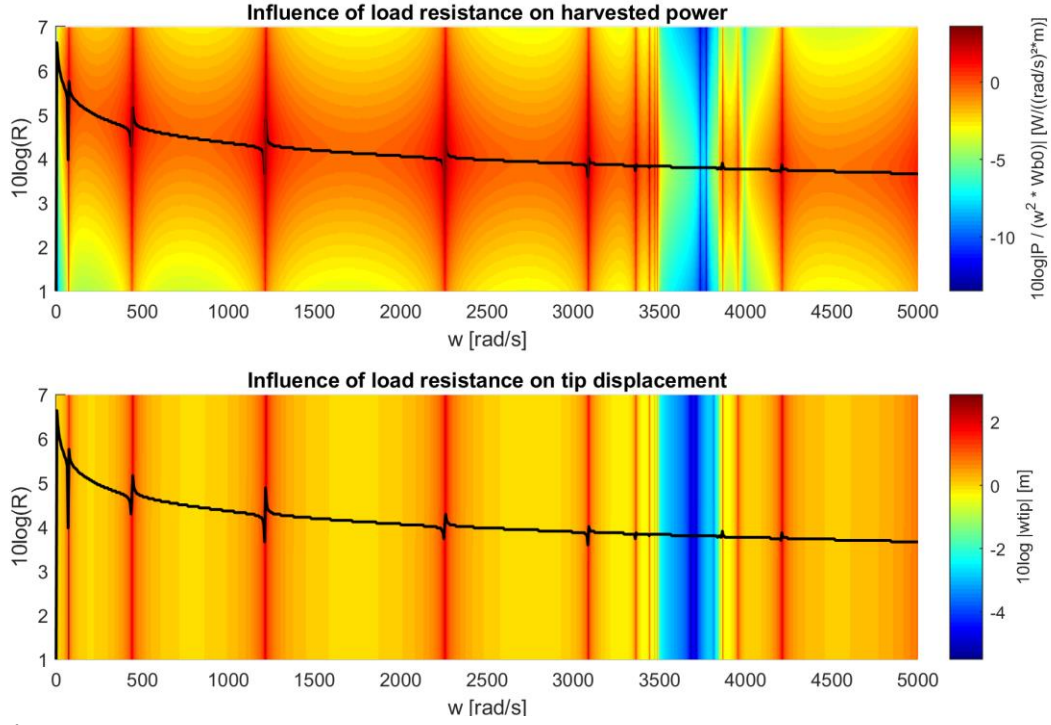


FIGURE 17: INFLUENCE VARYING LOAD ON POWER AND TIP DISPLACEMENT

7.7. Comparison to initial guess

We can now compare the power harvested with the power harvested via the initial guess. The two FRF's are displayed in figure 18. The general behavior of the cantilever clearly has not changed. One notable

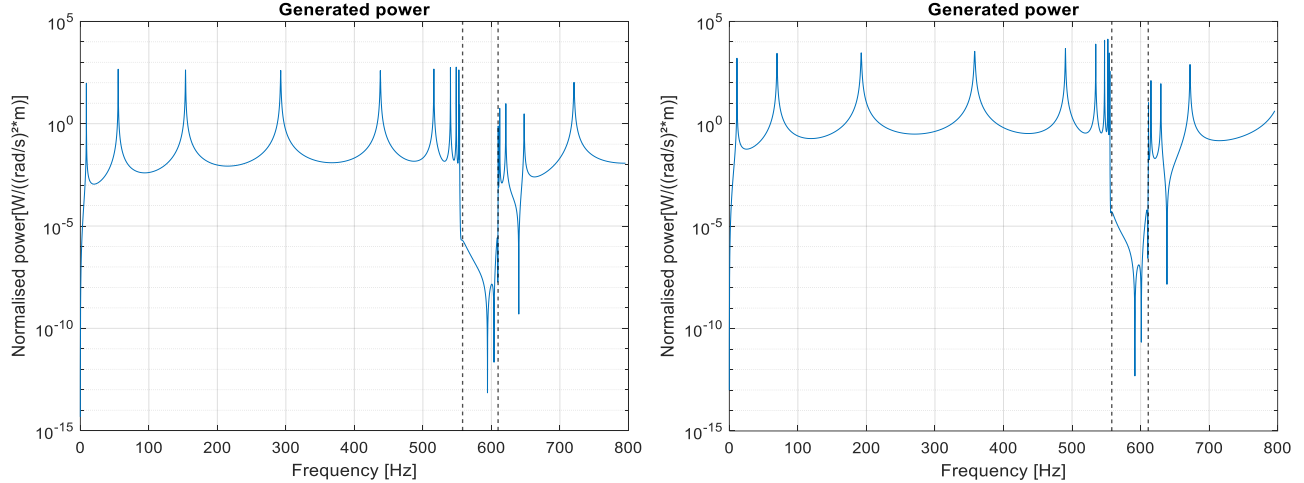


FIGURE 18: COMPARISON BETWEEN HARVESTED POWER WITH INITIAL GUESS AND OPTIMISED PARAMETERS

difference is that the generated power in the region near the bandgap, where it is desirable to harvest energy, has increased by one order of magnitude. As comparison, the beam parameters for the initial guess and after optimization are given in tables 6 and 7

Mass ratio	0,2
M_j [kg]	0,0025
N – resonator count	10
K_j [N/m]	3.07 E4
ξ [J]	≈0
̄e₃₁ [C/m²]	-10.4
̄e₃₃ [F/m]	13.3 E-9
̄c₁₁ [GPa]	61
ρ_p [kg/m³]	7750
R_L [ohm]	1000
H_p [m]	0.15 E-3

TABLE 6: INITIALLY GUESSED PARAMETERS

Due to adequate initial guesses, only the load resistance, piezopatch material and piezopatch thickness have been changed, and the spring-mass constant according to the added mass. This has, however, had a significant influence on the amount of energy that is able to be harvested in the targeted frequency region.

Mass ratio	0,2
M_j [kg]	0,0046
N – resonator count	10
K_j [N/m]	5.64 E4
ξ [J]	≈0
̄e₃₁ [C/m²]	-16.6
̄e₃₃ [F/m]	25.55 E-9
̄c₁₁ [GPa]	60.9
ρ_p [kg/m³]	7500
R_L [ohm]	10 000
H_p [m]	1.5 E-3

TABLE 7: PARAMETERS AFTER OPTIMISATION

8. Conclusion

A 2D beam with piezo electric elements in its entirety and mechanical resonators was simulated over a variety of parameter changes. A bandgap of 50Hz was formed at 558Hz as was targeted and thus cancelling out the fifth resonance frequency of the beam. This was achieved with resonators weighing only 20% of the beam including piezo elements. The bandgap was positioned by tuning mass and stiffness of the resonators. It was found that at least 10 resonators are needed for the cantilever to converge to a consistent bandgap at expected frequencies.

It was found through calculation and plots that the resonance frequencies could be influenced by changing stiffness and mass of the piezo elements. Further it was found that damping can work to smoothen the resonance peaks, while altering the load resistance showed no significant change to the deflections themselves.

Parameters for designing the cantilevered beam were optimized for power generation between 480Hz and 560Hz and it was found that a wide resonance frequency can be achieved through carefull tuning. With respect to an initial guess of beam parameters, several aspects were changed after optimization, including the load resistance, piezoelectric material and piezopatch thickness. While this considerably increases the weight of the beam, the mass ratio remained low, and structural integrity is provided. PZT-5H was used for the case study as it has a high piezo electric constant for orthogonal strain and electric fields.

9. Outlook

Having found that much of the potential of the piezo patches is lost due to mode cancellations the most pressing improvement for energy harvesting is to separate the Piezo patches into multiple smaller patches. At least as many patches as the highest order of mode shape that is harvested from is needed. Before designing the piezo setup it has been found to be important to evaluate exactly what mode shapes can be expected to be activated significantly.

Separate piezo patches could also be used as electrical resonators and by placing it next to the mechanical resonator bandgap the total bandgap can be enhanced significantly without increasing the weight (C Sugino, 2017). A non-linear study could be conducted either to widen resonance frequencies targeted for harvesting or to increase bandgap width. The examined non-linearities could come from material, damping, geometrical hardening or from bi-stable structures.

Furthermore, the applications of the structures could be studied. This would give a definite direction of the technical examination. Commonly mentioned applications are sensors in areas without easy power access like wings of windmills or airplanes. Another example use could be acoustics coupled with control, the project group has undertaken a case study for a hearing aid with the aim to minimize the mechanical feedback from the hearing aid speaker to the microphone. The microphone in a hearing aid is suspended with a hollow cantilever letting in sound from the surrounding world. By attaching piezo electric elements and with proper control it may prove to be possible to continually readjust the bandgap created by the piezo elements to whichever frequency is dominant in the immediate recording of the microphone. Other controllers could be applied.

References

- Braghin, F. (2019). *Smart Materials*. Milano: Politecnico De Milano.
- C Sugino, S. L. (2017). An investigation of electroelastic bandgap formation in locally resonant piezoelectric metastructures. *Smart Mater. Struct.*
- Charles Sherman, J. B. (2007). *Transducers and Arrays for Underwater Sound*. Springer Science+Business Media.
- Christopher Sugino, S. L. (2016). On the mechanism of bandgap formation in locally resonant finite elastic metamaterials . *JOURNAL OF APPLIED PHYSICS*.
- Erturk, A. (2019). Smart Structures and Devices Project Presentation Slides. Georgia Institute of Technology, Georgia, USA.
- Fleischer, C. (27. 05 2019). *autodesk.com*. Hentet fra Autodesk:
<https://www.autodesk.com/products/eagle/blog/piezoelectricity/>
- Inman, A. E. (2011). *Piezoelectric Energy Harvesting - Analytical Distributed-Parameter Electromechanical Modeling of Cantilevered Piezoelectric Energy Harvesters First Edition*. John Wiley & Sons.
- Inman, A. E. (2011). *Piezoelectric Energy Harvesting - Appendix C Modal Analysis of a Uniform Cantilever with a Tip Mass*. John Wiley & Sons, Ltd.
- Mehdizadeh, M. (22. 10 2009). Microwave/RF Applicators and Probes for Material Heating, Sensing, and Plasma Generation A Design Guide. *Science Direct*, s. 1-34.